Scientia Iranica A (2018) 25(4), 1931–1942

Sharif University of Technology
Scientia Iranica
Transactions A: Civil Engineering
http://scientiairanica.sharif.edu

Reservoir's geometry impact of three dimensions on peak discharge of dam-failure flash flood

A. Tahershamsi[a], F. Hooshyaripor[a,*], and S. Razi[b]

a. *Faculty of Civil and Environment Engineering, Amirkabir University of Technology, Tehran, Iran.*
b. *Department of Civil Engineering, Islamshahr Branch, Islamic Azad University, Tehran, Iran.*

Received 11 March 2016; received in revised form 22 August 2016; accepted 11 September 2017

KEYWORDS
Dam failure;
Failure ratio;
Peak-discharge;
Reservoir shape;
Cross-section index.

Abstract. Once a dam fails, large amount of water at rest in the reservoir burst into downstream river causing extensive inundation of areas, damage to properties, and loss of lives. The outflow hydrograph is affected by a variety of factors such as dam's properties, failure mode, and reservoir specification. This paper aims to analyze effects of the two latter factors on the peak outflow discharge by focusing on the relative size of the failed part employing failure ratio (a/A_0) and shape of the reservoir employing shape factor (S_f) and cross-section index (λ). In doing so, instantaneous experimental dam break and historical gradual failure were considered, and separate analyses were carried out. Results showed that a higher peak discharge is expected when S_f decreases or a/A_0 and λ increase. Based on the experimental and historical dam failure data, two distinct regression equations were developed and verified to estimate peak discharge. The sensitivity analysis demonstrated that peak discharge is highly sensitive to the changes of the failure ratio and shape factor; moreover, it is influenced by the cross-section index to some extent.

1. Introduction

Dams are constructed to provide societies with water for agriculture, industry, and household uses. Flood control, hydroelectric-power generation, and river navigation are other objectives of dam construction. However, adverse environmental and sociological impacts are expected if dams fail inadvertently. Based on the causes of failure and types of a dam, different failure modes are expected [1]. Non-rigid embankment dams, such as earth-fill and rock-fill dams, fail gradually during almost overtopping and piping, while rigid dams usually fail instantaneously as a result of overturning and sliding. In the instantaneous failure, it is assumed that the dam structure is removed suddenly and the stored water is released rapidly into the downstream valley. Such failure constitutes the worse condition, where the most potential damages are expected [1]. On the other hand, gradual failure occurs over a period of time and, in some cases, no shock wave may be developed. In this case, usually, a part of the dam body is breached while it is contrary to the gravity dams where total failure is more common when their stability is verified independently for each vertical monolith. However, there are many pieces of evidence of partial failure for several types of dams [2]. Regardless of the failure condition, a highly unsteady flow would follow the dam failure, and it propagates over the initial stream flow and brings severe flooding problems to the societies. Many factors, such as reservoir bathymetry, dam type and its materials, and height and volume of water behind the dam, can substantially affect the dam failure flow [2,3].

To manage flood risk and plan emergency action,

*. *Corresponding author.*
E-mail address: Hooshyarypor@yahoo.com (F. Hooshyaripor)

doi: 10.24200/sci.2017.4467

it is necessary to estimate the inundated areas and time of dam break wave arrival in residential areas. For this reason, outflow hydrograph of dam break is usually estimated and, then, routed to downstream river [2]. In this regard, an experimental study has been a useful approach to a better understanding of this complex phenomenon and reducing some of the involved uncertainties. However, they do not have the ability to control all variables and it is difficult and expensive to construct a complicated geometry in the laboratory. A numerical method is an alternative approach which has widely been used in dam break problems. Today, the proposed numerical techniques and computer software are able to correctly handle dam break flow features, e.g. discontinuities, high gradients near drying/wetting front, complex bed geometry, and source terms [4,5], and can provide values of the required variables over the computational domain. In this direction, the numerical solution to the Reynolds Averaged Navier Stokes (RANS) and the Shallow Water Equations (SWEs) has been frequently used [5]. It has been shown that 3D nature of the dam break flow close to the dam cannot be carefully captured when vertical acceleration is neglected [6]. At present, in order to simulate the failure of an actual dam considering the reservoir's real dimensions, numerical methods are time consuming; therefore, simpler methods are preferred to be applied by practical engineers. A conventional statistical method, on the other hand, is very fast and simple. It is based on the analysis of datasets from historical dam failures. This method is useful and applicable when a robust database containing high-quality data is available; hence, it has been frequently used in the case of gradual dam breach analysis. In this approach, the outflow peak discharge is described as a function of a number of quantities of dam and reservoir, e.g., water depth, storage volume, dam type and its erodibility, and the reservoir geometry. Eqs. (1) to (6) in Table 1 are some instances of such equations. Feizi et al. [3] and Wang et al. [6] evaluated some of these equations, and concluded that equation of Froehlich [7] has the best performance. However, it was mentioned that the overall performance of the equations is moderate.

Regarding Table 1, most of the equations associate the peak discharge with height and volume of the water behind the dam. However, some experimental and numerical researches [2,3,11,13] have demonstrated that reservoir bathymetry and failure geometry can also affect the amount of peak discharge. For instance, Ponce [13] defined the dimensionless peak-discharge ($\overline{Q_p}$) and reservoir shape factor (S_f) as follows:

$$\overline{Q_p} = Q_p / \left(B_b \sqrt{g H_b^3} \right), \tag{7}$$

$$S_f = \left(B_b H_b \right) / \left(B_d H_d \right), \tag{8}$$

where g is the gravity acceleration (m/s^2). Ponce [13] used historical embankment dam failure data to derive the best relation between both variables and found an inverse relationship between $\overline{Q}_p$ and S_f. Evaluating 24 embankment dam failures, Tahershamsi et al. [11] improved the shape factor as follows:

$$S_f = B_b B_d H_d / V_r. \tag{9}$$

Pilotti et al. [2] explored a wide range of natural reservoir's geometries and considered the reservoir bathymetry and failure size in their equation:

$$Q_p = \eta A_0 \sqrt{g H_0} \left[\sqrt{\lambda} \left(\frac{2\lambda + 1}{2\lambda} \right)^{2\lambda+1} \right]^{(-a/A_0)}, \tag{10}$$

Table 1. Empirical equations for peak discharge prediction from embankment dam failure.

Source	No. of case studies	Considered parameters	Equation[a]	Equation no.
[8]	21	Q_p, H_w	$Q_p = 19.1 H_w^{1.85}$	(1)
[9]	29	Q_p, V_w	$Q_p = 0.72 V_w^{0.53}$	(2)
[10]	23	Q_p, V_w, H_w	$Q_p = 1.154 (V_w H_w)^{0.412}$	(3)
[7]	22	Q_p, V_w, H_w	$Q_p = 0.607 V_w^{0.295} H_w^{1.24}$	(4)
[11]	24	$Q_p, V_r, B_b, H_b, B_d, H_d$	$Q_p = 0.026 B_b^{0.19} H_b^{1.5} \left(\frac{V_r}{B_d H_d} \right)^{0.81}$	(5)
[12][b]	93	Q_p, V_w, H_w	$Q_p = 0.0454 V_w^{0.448} H_w^{1.156}$	(6)

[a] The variables are: Q_p = Peak discharge (m^3/s);

H_w and V_w = Height (m) and volume (m^3) of water above the breach at the failure time;

V_r = Reservoir capacity (m^3); B_b = Breach top width (m); H_b = Breach maximum depth (m);

B_d = Dam top width (m); and H_d = Dam maximum height (m).

[b] V_w is used in Mm^3.

in which a/A_0 is failure ratio of the failure area (a) to the total wetted area of the dam (A_0), λ is cross-section index of the reservoir, while $A_0 = \delta H_0^{\lambda}$ (H_0 is water depth at the dam location and δ is a function of H_0 with specific value for a given cross-section), and η can be approximated as $\eta = 0.959(a/A_0)^{1.414}$.

Regarding the above-mentioned equations, each researcher has developed an equation based on limited involved parameters which cannot well describe the phenomenon; therefore, such equations are not reliable enough for dam failure risk analysis. Another criticism levelled at the equations points to the accuracy of the documented data. Indeed, techniques applied to determine some of the peak-discharges are undocumented, and some other peak-discharges have been measured at downstream locations far from the dams [14]. In addition, there are several reports in which several individuals presented different data for a specific failure event [15]. In spite of such uncertainties, empirical equations are still attractive to the practical engineers and are widely used in dam failure risk analysis to estimate the potential hazards associated with the structure failure [5]. A reliable empirical equation should be derived based on a robust database with more accurate, high-quality data. Otherwise, dam failure consequences could be very catastrophic and irrecoverable. This study follows two important objectives. The first is to apply experimental and numerical dam break simulations to investigate the effect of reservoir's geometry in three dimensions on the outflow hydrograph and developing a robust and reliable statistical equation to estimate peak discharge from an instantaneous dam break, which could be applied to concrete dam break risk analysis. This part will provide sufficient data measured by precise equipment, which may be instrumental for any other investigators. The second objective is to use reliable historical field data to derive a new statistical equation for peak discharge prediction from embankment dam failures with a particular focus on the most effective geometric and hydraulic parameters. In this study, to have a more reliable equation for peak discharge estimation, most of the known available dominant factors from the previous studies have been considered by applying dimensionless parameters and nonlinear multi-regression analysis.

2. Approach and methodology

According to the empirical equations (1) to (10), the peak discharge can be written as a function of the independent factors:

$$Q_p = f\left(g, B_d, H_d, B_b, H_b, V_r, \lambda\right). \tag{11}$$

Applying Π-Buckingham theorem [16], considering g and H_b as the repeating variables, we have the following non-dimensional relation:

$$f_1\left(\frac{Q_p}{\sqrt{gH_b^5}}, \lambda, \frac{B_d}{H_b}, \frac{B_b}{H_b}, \frac{H_d}{H_b}, \frac{V_r}{H_b^3}\right) = 0. \tag{12}$$

After some algebraic operations, Eq. (12) could be rewritten as follows:

$$\frac{Q_p}{B_b\sqrt{gH_b^3}} = f_2\left(\lambda, \frac{a}{A_0}, S_f, \frac{B_b}{H_b}, \frac{H_d}{H_b}\right). \tag{13}$$

Eq. (13) indicates that Q_p is a function of λ as an indicator of the reservoir cross-section, a/A_0 as representative of the failure dimensions, and S_f as representative of the reservoir length while it can be rewritten as $L_r \approx V_r/(B_dH_d) = B_b/S_f$. Non-dimensional parameters, B_b/H_b and H_d/H_b, are constant in this study; hence, they can be omitted from further analysis. Also, as shown by Pilotti et al. [2], $\overline{Q_p}$ can be improved as $\frac{Q_p}{B_b\sqrt{gH_b^3}}\left[\sqrt{\lambda}\left(\frac{2\lambda+1}{2\lambda}\right)^{2\lambda+1}\right]^{(a/A_0)}$; therefore, in total, we could summarize Eq. (13) as follows:

$$\overline{Q_p} = f_3\left(\frac{a}{A_0}, S_f\right). \tag{14}$$

In this study, to determine f_3 function, two sets of data, i.e., experimental dam break and historical dam breach data, will be applied, and separate equations will be developed using regression analysis. In the case of instantaneous dam break simulation, three categories of reservoir with different geometries are considered in the laboratory (Figure 1): wide rectangular, long rectangular, and trapezoidal (in plan view). Note that the cross-section of all the reservoirs is rectangular ($\lambda = 1.0$).

Due to some experimental limitations of the apparatus as well as high turbulent flow close to dam [3], calculation of Q_p at the dam location is not possible; therefore, Computational Fluid Dynamic (CFD) is applied. A CFD package based on the 3D numerical solution to RANS equations is tuned using the experimental data. Then, three experimental cases as representative of the three categories of the reservoirs' shape are selected to simulate dam break flow, numerically. These three cases have a similar reservoir's capacity. Based on the numerical simulation, the difference percentile between Q_p at the dam and any downstream point is calculated. These percentiles will be used for estimation of Q_p values of the other experimental cases at the dam where peak discharges are not possible to be measured by the apparatus. Then, the obtained peak discharges will be used to derive an equation with the shape factor and failure ratio as independent variables. In the case of gradual dam breach, historical data with respect to our case study are collected to develop another

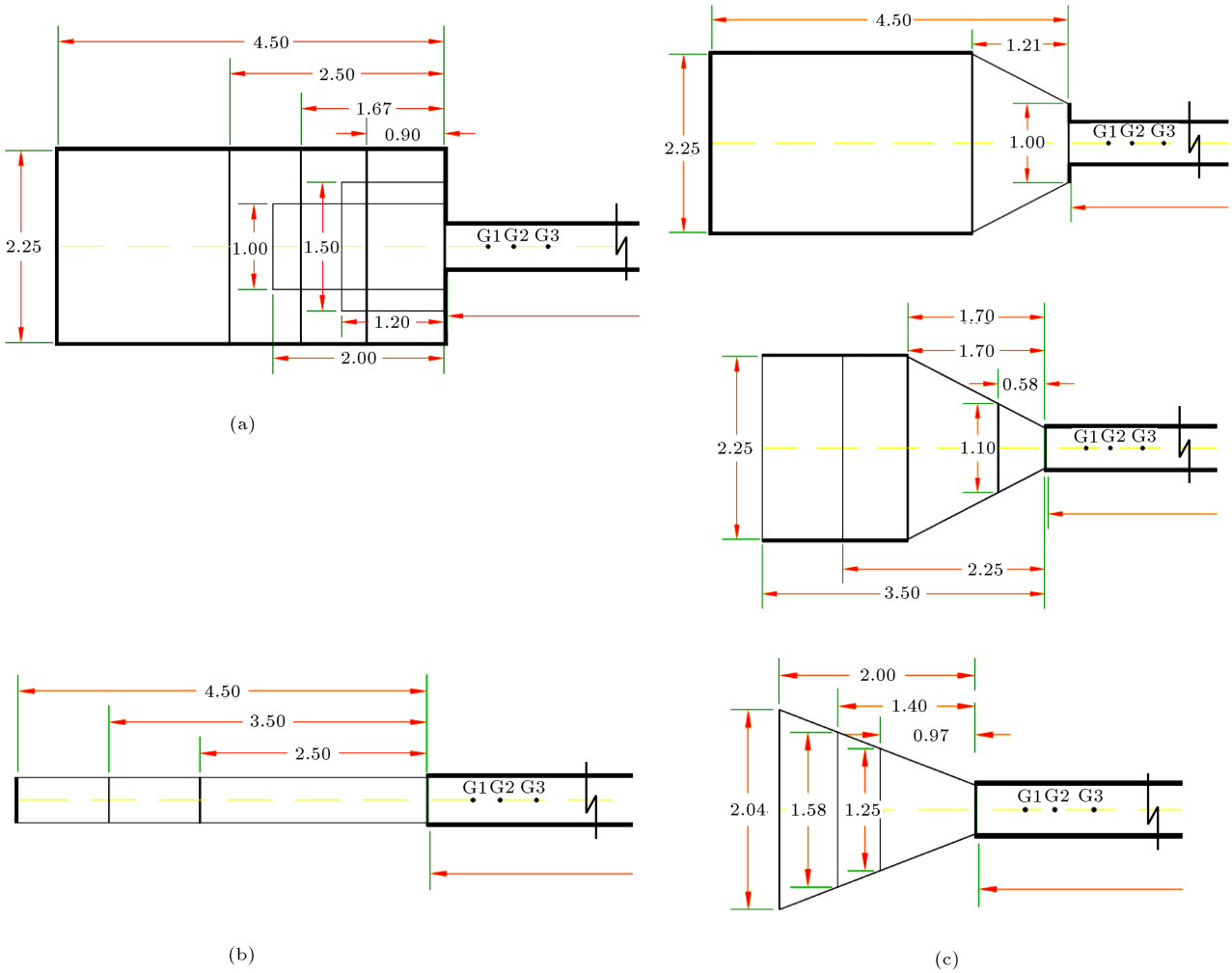

Figure 1. Plan view of (a) wide rectangular, (b) long rectangular, and (c) trapezoidal reservoir shapes (units in meter).

equation based on the regression analysis over the effective parameters. Finally, the obtained equations are compared with some of the available equations to evaluate their performances.

2.1. Experimental study

The experiments were carried out in the Hydraulics Laboratory of Civil Engineering Department, Amirkabir University of Technology, Iran, in which several reservoirs with different shapes in plan were examined Figure 1(a)-(c). The experimental setup includes three main parts: a rectangular reservoir at upstream, a rectangular flat and horizontal flume at downstream, and a gate installed in between (Figure 2).

To simulate the instantaneous dam break, the gate pulls up rapidly with the aid of a pneumatic jack [3]. The downstream flume is a 0.51 m wide, 0.7 m high, and 9.3 m long glass channel. The flume ends with a free overflow section. To minimize the interference of water and gate, the gate is made of a 10 mm thick plexiglas plate. The scale effect in a smooth prismatic and rectangular channel is insignificant if the initial water depth against the gate is $H_0 \geq 0.3$ m and that the dam break flow essentially follows the Froude similitude [17]. Accordingly, in all the tests, H_0 is considered to be 0.35 m or 0.4 m. The gate opening time in this study is $t_{op} = 0.14$ s. According to the criterion established by Vischer and Hager [18], the mentioned time shows that the dam break simulations can be considered instantaneous. Considering $H_0 = 0.35$ m:

$$t_{cr} = 1.25\sqrt{H_0/g} = 0.23 \text{ s}, \tag{15}$$

which is larger than t_{op}.

Four ultrasonic sensors and one Acoustic Doppler Velocimeter (ADV) were used for measuring the water level and velocity components, respectively. The ultrasonic sensors with response frequencies of up to 100 Hz were located at 0.5, 0.8, 1.2, and 5.5 m downstream the gate (respectively points G1, G2, G3, and G4 in Figure 2). The sensors were installed above the flume on a movable device mounted on a rail at the top of the model. Hence, no flow perturbation was

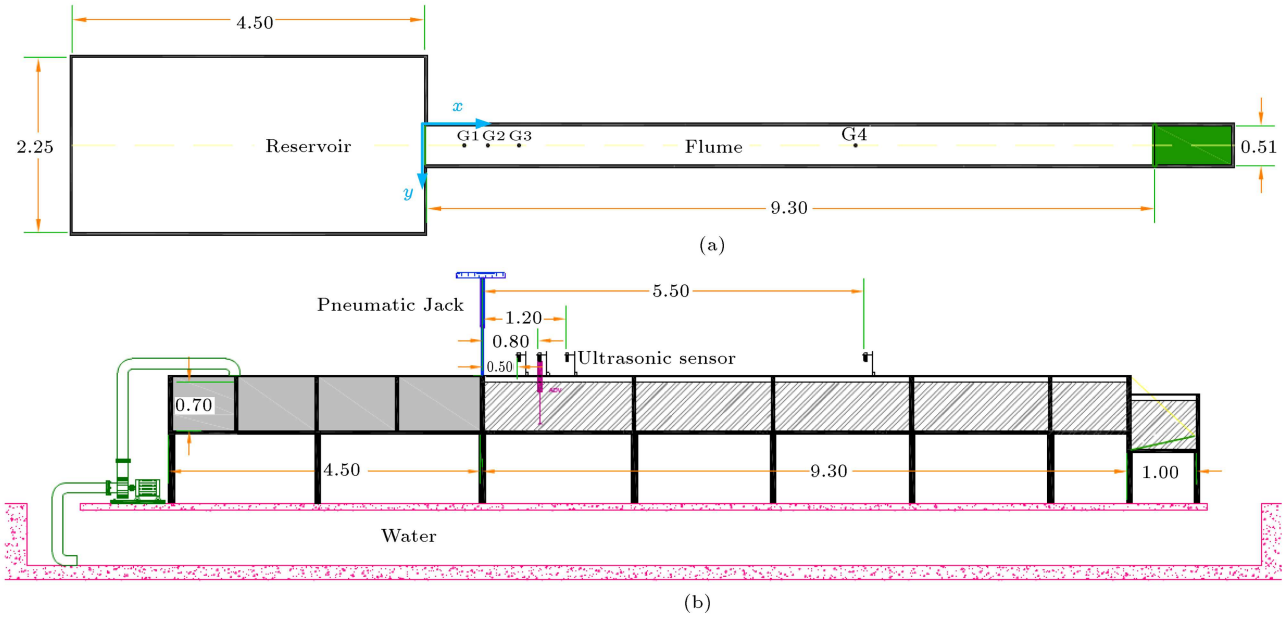

Figure 2. The experimental setup of (a) plan view and (b) longitudinal section.

created by them. To reduce the side wall boundary-layer effects, the measurement points were positioned at the flume centreline. Water level measurement has ±0.12 mm accuracy [3]. The ADV, mounted on the movable device on the top of the flume (Figure 2), has response frequencies of up to 50 Hz (SonTec MicroADV). This tool has been successfully used in dam break studies [3,19,20]. Small diameter of the ADV probe (6 mm) causes local and negligible perturbations in the flow [3,19].

2.2. Numerical study

To determine the flow characteristics at the gate and improve the design of process equipment, the 3D module of CFD package of fluent 6.3.26 was applied. Fluent has previously been applied and evaluated to simulate dam break problem [20]. The fluent software uses finite volume method to solve the governing integral equations. In this study, the so-called segregated solver was applied, so the governing equations were solved sequentially, i.e., segregated from each other. Various velocity-pressure coupling algorithms were examined along with a Volume Of Fluid (VOF) scheme for the phase interface capturing. As the governing equations are non-linear and coupled, a number of iterations of the solution loop must be performed to obtain a converged solution. Moreover, various grid sizes, time steps, bed roughness values, and turbulence models were examined to obtain the most realistic results from the solver.

2.3. Historical case studies

Wahl [15] identified numerous equations developed since 1984 based on the analyses of historical case studies comprising 20 to 60 dam failures and documented a valuable database containing 108 failures. However, there are many instances of significant discrepancies between datasets reported by different investigators. Ponce [13] evaluated the documented cases and presented a valuable database. Taher-Shamsi et al. [11] compared the databases of Ponce [13] and Wahl [15] and selected 24 datasets reported directly from original sources, or their reported times were closer to the event time. This database is used in the present study (Table 2). The table also includes five other cases from different references to be applied to verification of the results and sensitivity analysis.

3. Results and Discussion

3.1. Experimental results

In the physical model, the gate plays the role of the dam. Once the gate is opened, the still water at the reservoir abruptly flows downstream, and the ultrasonic sensors at the pre-determined locations record the water level. Figure 3(a) shows the temporal variations of water level at G2 for the three representatives (in the category of the wide rectangular reservoirs, the reservoir with 0.9 m length and 2.25 m width (Case A); in the category of the long rectangular reservoirs, the reservoir with 4.5 m length (Case B); in the category of the trapezoidal ones, the reservoir with 1.7 m length and 2.25 m end width (Case C)). Note that the volumes of the reservoirs are not the same; however, the three representatives have the closest capacities.

Due to the instrumental restrictions, the nearest point to the gate for installing the ADV probe is G1. Regarding the water level variation in a point, the

Table 2. Historical case study data and the dimensionless parameters.

No.	Dam/reservoir	V_r (m-m^3)	H_d (m)	B_d (m)	H_b (m)	B_b (m)	Q_p (m^3/s)	a/A_0	S_f	$\overline{Q_p}$	Source
1	Armando de Salles Oliveira	25.9	35	660	35	167.64	7195	0.254	0.15	0.09	
2	Baldwin Hills	1.11	48.77	167.64	48.77	121.92	141.58	0.727	0.898	0.003	
3	Break Neck Run	0.0493	7.0	63	7.0	30.48	9.2	0.484	0.273	0.009	
4	Dells	13	17.98	292.61	17.98	112.77	5434.9	0.385	0.046	0.323	
5	Euclides da Cunha	13.6	53	304.8	53	131.06	1005.2	0.43	0.156	0.011	
6	Elk City	0.74	9.14	259.08	9.14	45.72	608.79	0.176	0.146	0.191	
7	Dam near Frankfurt	0.351	9.75	120	9.75	9.45	79.28	0.079	0.032	0.097	
8	Frenchman	8.64	12.19	884	12.19	243.84	1602.7	0.276	0.304	0.069	
9	Goose Creek	10.6	6.09	701.04	3.96	30.48	492.7	0.028	0.012	0.678	
10	Hatchtown	14.8	19.81	237.74	19.8	36.57	1970.8	0.154	0.011	0.236	
11	Hatfield	12.2	6.7	137.16	6.7	91.44	3397.9	0.667	0.007	1.539	
12	Hemet	8.63	6.09	83.21	6.09	30.48	1600	0.366	0.002	1.742	[11]
13	Horse Creek	20.9	16.76	182.88	12.8	60.96	3883.2	0.254	0.009	0.605	
14	Kelly Barnes	0.493	7.92	152.4	7.92	137.16	549	0.9	0.336	0.171	
15	Knife Lake	9.86	6.096	60.96	6.096	12.19	1098.66	0.2	0.001	2.438	
16	Lake Avalon	7.77	14.63	420.6	14.63	137.16	2321.9	0.326	0.109	0.144	
17	Lake Latonka	1.59	13.11	701	13.11	33.53	294.48	0.048	0.194	0.063	
18	Mammoth	13.5	21.34	48.77	21.34	9.14	2520.1	0.187	0.0007	1.122	
19	Nanaksagar	210	15.85	3218.6	15.85	45.72	9709.5	0.014	0.011	1.093	
20	Puddingstone	0.616	15.24	251.46	10.67	91.44	283.2	0.255	0.569	0.039	
21	Sherburne	0.0752	10.36	91.44	10.36	45.72	14.2	0.5	0.576	0.006	
22	Sinker Creek	3.33	21.34	335.28	21.34	91.44	926	0.273	0.196	0.046	
23	Teton	308	92.96	945	79.55	45.72	46786.5	0.041	0.013	0.484	
24	Whitewater Brook	0.518	18.9	137.16	6.1	6.4	70.79	0.015	0.032	0.239	
Historical dam breach data for verification of the results											
1	Big Bay Dam	17.5	15.6	576.07	15.6	96	4160	0.167	0.049	0.275	[21]
2	Schaeffer Reservoir	4.44	30.48	335.3	27.43	210.31	4629.8	0.564	0.484	0.097	[10]
3	Johnstown (South Fork Dam)	18.9	38.1	283.5	24.4	128	8500	0.289	0.073	0.250	[15]
4	Shimantan	117	25.8	500	25.8	446	30000	0.892	0.049	0.485	[22]
5	Banqiao	607.5	29.5	2000	29.5	372	78100	0.186	0.036	0.525	

velocity components are recorded at several depths (with 10 mm interval from the minimum distance of ADV installation to the channel bottom). Note that every test is repeated at least three times to ensure that the results are reliable and accurate. Then, based on the velocity values at different depths, depth averaged velocity in each time step is calculated as:

$$U = \frac{1}{Z}\sum_{i=1}^{n} u_i.\Delta z_i,$$

where u_i is the measured velocity, n is number of special steps, and $Z = \sum_{i=1}^{n} \Delta z_i$ is range of velocity measurement. Following this procedure for all time steps, the time evolution of the depth-averaged velocity is calculated. Figure 3(b) illustrates the obtained results at point G2. By acquiring the average velocity and water level at each time step, the flow rate is determined as $Q = B.U.H$, where B is the width of the flume (= 0.51 m) and H is flow depth at any point of measurement at time t. Figure 3(c) shows the calculated flow rate at point G2 for the representative reservoirs. This figure shows the impact of reservoir's geometry on the outflow hydrograph. Although the volume of water in the reservoirs is almost equal, failure of the wide rectangular reservoir results in a higher peak discharge in an earlier time, and the reservoir gets empty faster than two other reservoirs do. It is obvious that the long rectangular reservoir's hydrograph has a

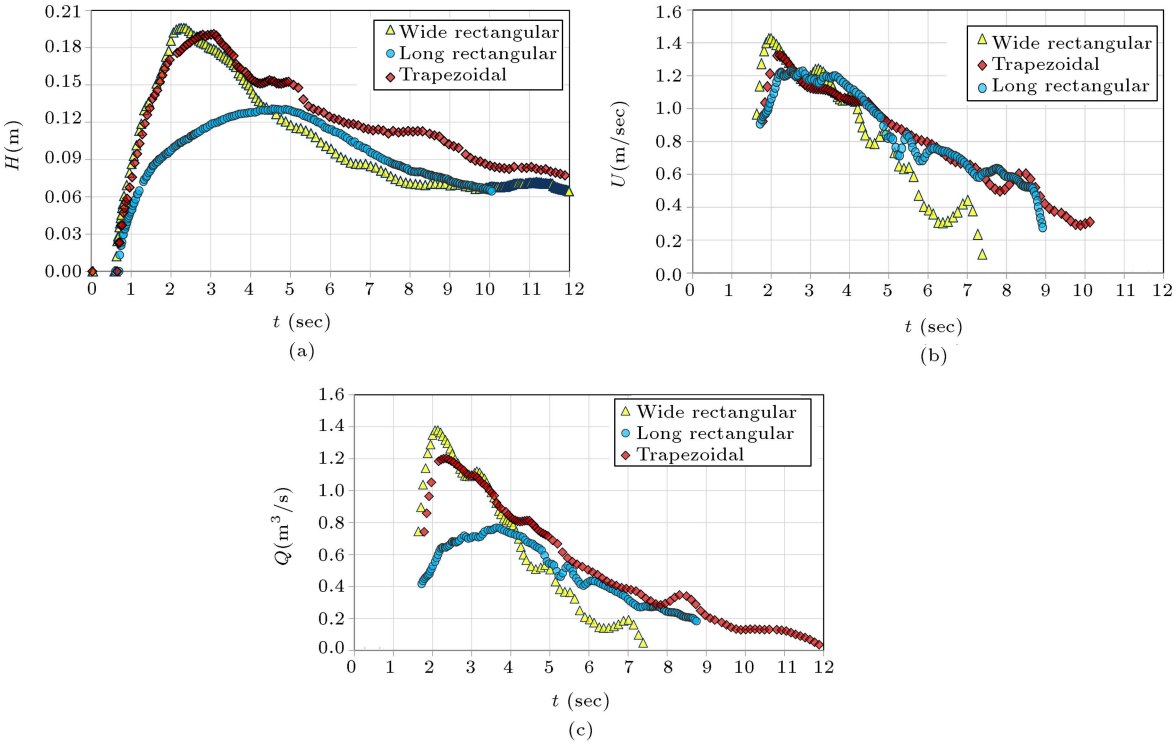

Figure 3. Flow characteristics at point G2 of (a) water level, (b) average velocity, and (c) flow rate.

relatively mild increasing trend of the peak discharge of lower value as compared to the other reservoirs. It means that the geometry of the reservoir is very important in dam failure analysis. As can be seen, Q_p of the wide rectangular reservoir is the highest ($= 0.138$ m^3/s), with trapezoidal and long rectangular reservoirs containing respective peak discharges of 0.12 and 0.077 m^3/s being almost the highest. The value of Q_p for all the examined reservoirs is calculated and presented in Table 3.

3.2. Numerical results

In the numerical simulations, water is initially confined to the reservoir by the presence of a dam at the flume entrance. At time $t = 0$, the dam is removed instantaneously, and the water starts to flow to the downstream. Flow characteristics are monitored at 0.5 m, 0.8 m, and 1.2 m downstream the gate and also at the gate location. To investigate the sensitivity to the grid size and the accuracy of the results, different grid sizes are examined. Considering both the accuracy and computational cost, the grid size of 30 mm is found to be suitable for the purpose of this study. Considering $\Delta x = 30$ mm and $\Delta t = 0.003$ s, the sensitivity analyses are carried out for the turbulence model, bed roughness value, and pressure-velocity coupling algorithm. Accordingly, the $k-\varepsilon$ turbulence model [23] is used to account for turbulence, the velocity pressure coupling is resolved via a PISO type, and the value of bed roughness is considered to be 0.01 mm. In addition, the PRESTO pressure discretization scheme and the first-order upwind momentum and turbulent kinetic energy discretization scheme are applied. Convergence is reached when the normalized residual of each variable is in the order of 0.001. Moreover, the free surface is defined by a value of 0.5 for VOF. In order to verify the adjusted numerical model, at first, the long rectangular reservoir of 4.5 m long (Case B) is simulated in fluent. Figure 4 compares the numerical and experimental results at downstream stations. As can be seen, the numerical results have good agreement with the experimental data where the average RMSE and AE values for water level simulation are 8.22 mm and 5.72%, respectively. Then, the model is run again for representatives of two other categories of reservoirs (Cases A and C).

3.3. Data analyses

In the experimental setup, the breach width is equal to the channel width ($B_b = B$) (see Figure 2) and dam height is equal to the height of water behind the gate ($H_d = H_0$); therefore, the relation of shape factor (Eq. (9)) can be transformed into $S_f = BB_dH_0/V_r$. The values of S_f, a/A_0, and Q_p for historical case studies and different experimental models are calculated and presented in Tables 2 and 3, respectively. In addition, Table 3 includes the experimental data obtained from Feizi et al. [3] and Mirhoseini [24]. In Table 3, rows 1, 8, and 16 are related to the representative reservoirs of Cases A, B, and C, respectively. The

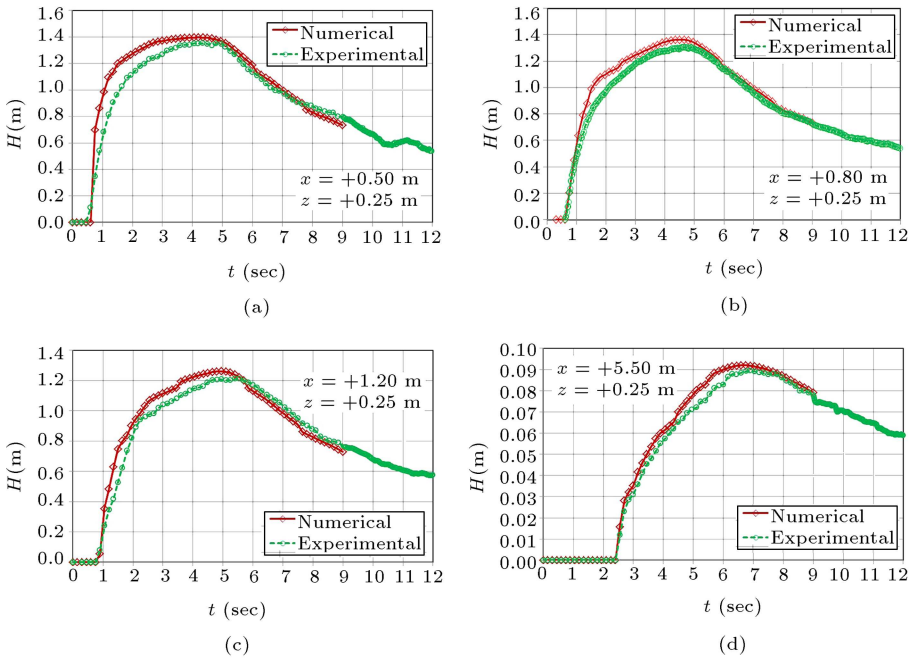

Figure 4. Verification of the numerical model for long rectangular reservoir of 4.5 m length at points (a) G1, (b) G2, (c) G3, and (d) G4 for temporal variation of water level.

Table 3. Values of the dimensionless parameters for experimental cases (in all cases $\lambda = 1.0$).

Reservoir shape	No.	Ref.	V_w (m^3)	$H_d = H_b = h_0$ (m)	B_d (m)	$B_b = b$ (m)	Exp. Q_p at G2 (m^3/s)	Num. Q_p at G2 (m^3/s)	Exp. Q_p at the gate (m^3/s)	S_f	a/A_0	$\overline{Q_p}$
Wide rectangular	**1**	**Fig. 1(a)**	**0.81**	**0.4**	**2.25**	**0.51**	**0.138**	**0.113**	**0.150**	**0.567**	**0.227**	**0.597**
	2	Fig. 1(a)	1.503	0.4	2.25	0.51	0.171		0.227	0.305	0.227	0.557
	3	Fig. 1(a)	2.25	0.4	2.25	0.51	0.179		0.238	0.204	0.227	0.584
	4	Fig. 1(a)	4.05	0.4	2.25	0.51	0.253		0.336	0.113	0.227	0.825
	5	Fig. 1(a)	0.80	0.4	1.0	0.51	0.15		0.199	0.255	0.510	0.69
	6	Fig. 1(a)	0.72	0.4	1.5	0.51	0.098		0.130	0.425	0.340	0.367
	7	[3]	0.712	0.4	2.0	0.51	0.123		0.163	0.573	0.255	0.415
Long rectangular	**8**	**Fig. 1(b)**	**0.803**	**0.35**	**0.51**	**0.51**	**0.077**	**0.076**	**0.098**	**0.113**	**1.0**	**1.011**
	9	Fig. 1(b)	0.714	0.4	0.51	0.51	0.082		0.106	0.146	1.0	0.685
	10	Fig. 1(b)	0.51	0.4	0.51	0.51	0.069		0.089	0.204	1.0	0.567
Trapezoidal	11	Fig. 1(c)	0.187	0.4	0.51	0.51	0.045		0.049	0.557	1.0	0.376
	12	[24]	0.341	0.4	0.51	0.51	0.073		0.079	0.305	1.0	0.61
	13	[24]	0.585	0.4	0.51	0.51	0.081		0.088	0.178	1.0	0.676
	14	[3]	0.720	0.4	0.51	0.51	0.115		0.125	0.145	1.0	0.96
	15	[24]	1.020	0.4	0.51	0.51	0.128		0.139	0.102	1.0	1.069
	16	**Fig. 1(c)**	**0.938**	**0.4**	**0.51**	**0.51**	**0.12**	**0.135**	**0.147**	**0.111**	**1.0**	**1.091**
	17	Fig. 1(c)	0.787	0.4	1	0.51	0.128		0.139	0.259	0.510	557
	18	[24]	1.658	0.4	0.51	0.51	0.133		0.145	0.063	1.0	1.111
	19	Fig. 1(c)	2.558	0.4	0.51	0.51	0.192		0.209	0.041	1.0	1.604
	20	Fig. 1(c)	3.748	0.4	1	0.51	0.235		0.250	0.054	0.510	1.081

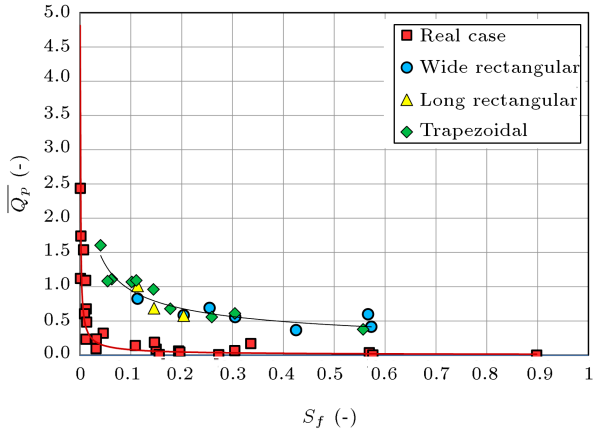

Figure 5. Dimensionless peak discharge versus shape factor values.

value of λ for all the historical cases is considered to be 1.0, because B_d is on average 20 times greater than H_d; therefore, the reservoir cross-section is supposed to be rectangular. The failure ratio is calculated based on the simplifying assumptions: (1) The failure is considered to be rectangular with width of B_b and height of H_b; (2) The dam cross-section is also supposed to be rectangular with width of B_d and height of H_d. Thus, a/A_0 is equal to $(B_bH_b)/(B_dH_d)$, which is equivalent to Eq. (8).

Figure 5 illustrates the dimensionless peak discharges versus the shape factor values. In the figure, two different curves are distinguished for the experimental and natural reservoirs.

As can be seen, for a specific shape factor value, $\overline{Q_p}$ value pertaining to the experimental reservoirs, which represent the instantaneous dam failures, is on average 8.75 times more than that of the gradual dam failures. This difference is due to the higher peak discharge value of the experimental reservoirs [3]. According to Figure 5, peak discharge increases when the shape factor decreases. Considering $L_r \approx V_r/(B_dH_d) = B_b/S_f$, for a constant failure width, the shape factor decreases by increasing the reservoir capacity introducing a longer reservoir. Therefore, for a given V_r, the longer reservoirs will produce a higher peak discharge. Figure 5 also illustrates that the increasing rate of peak discharge by reducing shape factor from 0.1 to zero is very high; thus, dam failure analysis is very important in this range of shape factors. In Figure 5, the corresponding curve of real dam breach data lies below the experimental curve. It means that, for a specific shape factor, peak discharge of an embankment dam failure is expected to be less than that of a concrete dam subjected to instantaneous dam failure. Conversely, a smaller peak discharge will be expected when someone uses a model for predicting an instantaneous dam break peak discharge, while it has been derived from the historical embankment dam failure data, and vice versa. In such conditions, the models will be underestimated or overestimated. Hence, the main reason for moderate performance of the statistical equations described by Feizi et al. [3] is the application of the equations derived from real cases of embankment dam failures for predicting the instantaneous experimental peak discharges.

By applying Eq. (14), the relations between the variables for experimental and real cases are determined as Eqs. (16) and (17), respectively:

$$\overline{Q_p} = 0.348{S_f}^{-0.455}(a/A_0)^{0.098}, \tag{16}$$

$$\overline{Q_p} = 0.134{S_f}^{-0.408}(a/A_0)^{0.207}. \tag{17}$$

Eqs. (16) and (17), with R^2 value more than 0.79, indicate that there is a direct relation between a/A_0 and $\overline{Q_p}$; therefore, a higher peak discharge is expected from a total dam failure in comparison with partial dam failure. The effect of failure ratio is much stronger in the case of historical dam breach data. Assuming $g = 9.806$ m/s^2 and full depth breach where the breach develops over the total height of the embankment ($H_b = H_d$), by substituting the dimensional parameters in Eq. (17), we have:

$$Q_p = 0.42\left(\sqrt{\lambda}\left(\frac{2\lambda+1}{2\lambda}\right)^{2\lambda+1}\right)^{-(a/A_0)} B_d^{-0.62}H_d^{1.09}B_b^{0.8}V_r^{0.41}. \tag{18}$$

3.4. Verification and sensitivity analysis

In order to evaluate the performance of the derived statistical equations in comparison with those already developed by other researchers, the datasets of five embankment dams comprising Big Bay Dam, Schaeffer Reservoir, Johnstown (South Fork Dam), Shimantan, and Banqiao are used. The Big Bay Dam of approximately 576 m long and 15.6 m high failed through piping in the vicinity of the principal spillway in 2004, 12 years after construction. A peak-discharge outflow of 4,160 m^3/s was estimated due to the embankment dam failure [21]. The Schaeffer reservoir, in Colorado, failed in 1921 which caused a severe flooding in downstream areas. Due to the failure, about 4.44 Mm^3 of water was released into Beaver Creek within 30 minutes with Q_p of 4,629.8 m^3/s [10]. Johnstown Flood due to the failure of the South Fork Dam upstream of the town of Johnstown, Pennsylvania occurred in 1889. The dam failure unleashed a torrent of 18.9 Mm^3 water from the reservoir with a peak discharge of 8,500 m^3/s [15]. In Henan, a province of China, Shimantan and Banqiao Dams failed in 1975; moreover, through the failure, flood with peak discharge of respectively 30,000 and 78,100 m^3/s occurred [22]. More details are available in Table 2.

Table 4. Performance of the empirical relations for peak discharge estimation.

No.	Dam/reservoir name	Estimated Q_p (m^3/s)						
		Eq. (1)	Eq. (4)	Eq. (5)	Eq. (6)	Eq. (10)	Eq. (16)	Eq. (17)
1	Big Bay Dam	3078	2508	1786	1911	6445	17368	4775
2	Schaeffer Reservoir	8745	3370	1434	1985	36033	21795	7621
3	Johnstown	7042	4468	3383	3317	19574	34422	10239
4	Shimantan	7808	8198	17681	8006	58293	83804	27662
5	Banqiao	10005	15737	23146	19552	72909	199037	54583
	RMSE (m^3/s)	32093	29614	25352	28109	19705	61093	10685
	AE (%)	–23.09	–53.38	–59.55	–64.09	190.23	265.48	12.39
	R^2	0.57	0.99	0.84	0.99	0.78	0.99	0.96

Using these datasets, the values of a/A_0 and S_f parameters are calculated for each of the embankment dams to be used for the estimation of peak-discharge value. Table 4 contains the results of some of the existing equations as well as the new derived equations.

Quantitative comparison of the results is done in terms of three statistical indices: RMSE, AE, and R^2. According to the results, RMSE value of Eq. (17) is 10,685 m^3/s, while the average value of Q_p corresponding to the five embankment dams is 25,077 m^3/s. The other relations have RMSE value more than 20,000 m^3/s where Eq. (16), as expected to be overestimating for gradual failures, has high RMSE value of 61,093 m^3/s, i.e., approximately 2.5 times more than average Q_p. On the other hand, AE index of Eq. (17) (= 12.39%) is more satisfactory than those of the other equations. In addition, Eqs. (1) and (4)-(6) are underestimated. Referring to the third index, the value of R^2 is acceptable in all cases; out of the relations, Eqs. (4), (6), and (16) have R^2 value of 0.99. Overall, Eq. (17) comes out as the most acceptable relation in terms of accuracy with the lowest RMSE and AE values and satisfactory high coefficient of determination. Moreover, Eq. (16), derived from instantaneous experimental dam break data, is highly overestimated for embankment dam failures and is not recommended to be used for gradual dam failure; however, it is suitable for sudden dam break analyses. Besides, Eq. (1) has very low correlation, and the performances of the other equations are moderate. Note that the predicted Q_p value for Banqiao Dam by Eq. (17) is very close to that calculated by Froehlich [14] as twice the average outflow rate over a 6-h period (56,300 m^3/s).

To determine how different values of the independent parameters impact the peak discharge, a sensitivity analysis was conducted on the effective parameters considering Shimantan Dam breach data. Shimantan Dam was selected due to good performance of Eq. (17) for its peak discharge estimation. The analysis was conducted in the possible range of the independent parameters where λ varies between 1 and 2; a/A_0 and S_f can take values greater than zero, and based on Table 2, S_f is typically less than one. Figure 6 presents the sensitivity of the peak discharge calculated by Eq. (17) to variations of S_f, a/A_0, and λ, separately.

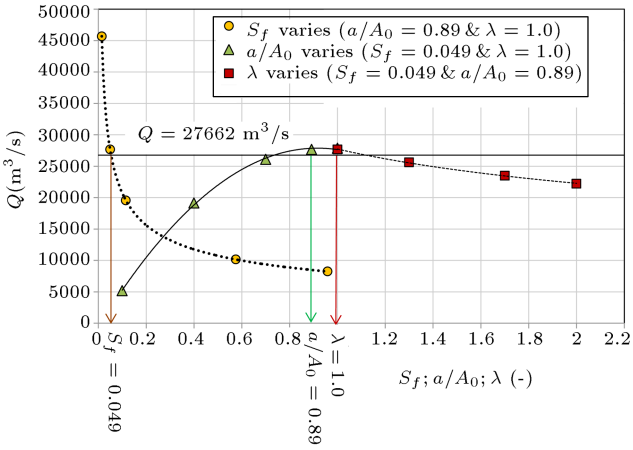

Figure 6. Sensitivity of peak discharge to the effective parameters' variation.

The three independent parameters are on the horizontal axis, while the calculated peak discharge is on the vertical axis. Figure 6 shows that failure ratio has significant influence on the magnitude of peak discharge value; typically, Q_p for failure ratio of 0.1 could be five times less than that for what actually happened in $a/A_0 = 0.89$. Shape factor, as shown in the figure, has an inverse effect on the peak discharge, such that Q_p may decrease to a little more than one third of the actual value if shape factor was 10 times larger than the actual current one. More shape factor could be interpreted as a reservoir with less capacity or more length or greater breach width. Finally, reservoir's cross-section index has inverse influence on the peak discharge, yet not as much as the two other parameters. As can be shown, the rectangular reservoir ($\lambda = 1.0$) leads to a higher peak discharge, compared to parabolic and triangular reservoir ($\lambda = 2.0$). For

Shimantan Dam failure, the peak discharge reduced by 20% if the cross-section was parabolic or triangular. Note that λ is much more controversial in the mountain reservoirs where different cross-sections can be distinguished: triangular cross-section in the upstream tributaries reaches the rectangular cross-section in the downstream; however, for the erodible dams, which are generally constructed in the plains, cross-section is usually rectangular. Figure 6 demonstrates that failure of the Shimantan Dam with $\lambda = 1.0$ and a/A_0 close to 1 due to overtopping can imply the reservoir being at the highest level (the least possible S_f value) and can be considered as the most catastrophic condition of failure imaginable.

4. Conclusion

This paper focused on the impact of reservoir geometry and failure size on the flash flood's peak discharge due to a dam failure. The experimental approach was employed to simulate instantaneous dam break, and data mining approach using historical event data was considered for embankment dam breach analysis. In the first approach, 14 reservoirs with different geometries in three categories of wide and long rectangular and trapezoidal shapes were considered in the laboratory, and instantaneous dam break was examined. Moreover, a 3D numerical package was tuned to analyze the flow characteristics at the dam location. The effective parameters in the peak discharge were distinguished by literature review; then, they were summarized in three dimensionless factors: shape factor to specify the reservoir geometry, cross-section index of the reservoir, and failure ratio to specify the failure size. Results showed that shape factor and failure ratio have a significant impact on the outflow hydrograph. Specifically, considering the smaller shape factor or more failure ratio, the higher peak discharge is expected. In the next step, regression analysis was used to derive simple equations for peak discharge estimation from instantaneous and gradual dam failures. Verification results indicated that employing failure ratio for the analysis could promote the performance of the regression model. Overall, in terms of risk assessment, the reservoirs with smaller shape factor and greater failure ratio will provide a higher peak-discharge. Based on the results, dam failure risk analysis is strongly proposed when the reservoir's shape factor is less than 0.1. Moreover, total failure ($a/A_0 = 1.0$) is the most catastrophic condition resulting in the largest peak discharge and the fastest mode of the reservoir emptying. However, most of the constructed dams in the world are non-rigid and partial failure is more probable in the nature. Since the failure ratio is an uncertain parameter depending on many structural and hydrologic factors, dam failure risk analysis needs establishing uncertainty analysis techniques, requiring further studies.

Nomenclature

a	Failure area (m^2)
A_0	Reservoir cross-section area at the dam location (m^2)
a/A_0	Failure ratio
B	Flume width (m)
B_b	Breach top width (m)
B_d	Dam top width (m)
g	Gravity acceleration (m/s^2)
H	Flow depth (m)
H_b	Breach maximum depth (m)
H_d	Dam height (m)
H_w	Water depth above the breach at failure time (m)
H_0	Water depth at the dam/gate location (m)
L_r	Dimensionless length of the reservoir
Q_p	Peak discharge (m^3/s)
$\overline{Q_p}$	Dimensionless peak-discharge
S_f	Shape factor
t_{op}	Gate opening time (s)
t_{cr}	Vischer and Hager time criterion (s)
U	Average velocity (m/s)
V_r	Reservoir capacity (m^3)
V_w	Water volume above the breach at failure (m^3)
Z	Range of velocity measurement (m)
RMSE	Root Mean Square Error
AE	Average Error
R^2	Coefficient of determination
Δx	Length interval (m)
Δt	Time interval (s)
λ	Reservoir's cross-section index
δ	Parameter for power-type expression of reservoir cross-section
η	Coefficient function in Pilotti equation

References

1. Singh, V., *Dam Breach Modelling Technology*, Kluwer Academic Publishers (1996).
2. Pilotti, M., Tomirotti, M., Valerio, G., and Bacchi, B. "Simplified method for the characterization of the hydrograph following a sudden partial dam break",

Journal of Hydraulic Engineering, **136**(10), pp. 693-704 (2010).

3. Feizi Khankandi, A., Tahershamsi, A., and Soares-Frazão, S. "Experimental investigation of reservoir geometry effect on dam-break flow", *Journal of Hydraulic Research*, **50**(4), pp. 376-387 (2012).
4. Aliparast, M. "Two-dimensional finite volume method for dam-break flow simulation", *International Journal of Sediment Research*, **24**, pp. 99-107 (2009).
5. Lohrasbi, A. and Pirooz, M.D. "Dam break model with Eulerian equations using mapping technique", *Scientia Iranica*, **23**(3), pp. 876-881 (2016).
6. Wang, B., Zhang, T., Zhou, Q., Wu, C., Chen, Y., and Wu, P.A. "Case study of the Tangjiashan landslide dam-break", *Journal of Hydrodynamics*, **27**(2), pp. 223-233 (2015).
7. Froehlich, D.C. "Peak outflow from breached embankment dam", *Journal of Water Resources and Planning Management*, **121**(1), pp. 90-97 (1995).
8. USBR, *Guidelines for Defining Inundated Areas Downstream from Bureau of Reclamation Dam*, Reclamation Planning Instruction No 82-11, US Department of the Interior, Bureau of Reclamation, Denver, 25 (1982).
9. Evans, S.G. "The maximum discharge of outburst floods caused by the breaching of man-made and natural dams", *Canadian Geotechnical Journal*, **23**(4), pp. 385-387 (1986).
10. Macdonald, T.C. and Langridge-Monopolis, J. "Breaching characteristics of dam failures", *Journal of Hydraulic Engineering*, **110**(5), pp. 567-586 (1984).
11. Taher-Shamsi, A., Shetty, A.V., and Ponce, V.M. "Embankment dam breaching: Geometry and peak outflow characteristics", *Dam Engineering*, **14**(2), pp. 73-87 (2003).
12. Hooshyaripor, F., Tahershamsi, A., and Golian, S. "Application of copula method and neural networks for predicting peak outflow from breached embankments", *Journal of Hydro-environment Research*, **8**(3), pp. 292-303 (2014).
13. Ponce, V.M., *Documented Cases of Earth Dam Breaches*, San Diego State University, SDSU Civil Engineering Series, No 89149 (1982).
14. Froehlich, D.C. "Predicting peak discharge from gradually breached embankment dam", *Journal of Hydrologic Engineering* (In Press). DOI: 10.1061/(ASCE)HE.1943-5584.0001424
15. Wahl, T.L., *Prediction of Embankment Dam Breach Parameters, a Literature Review and Needs Assessment*, Rep No DSO-98-004, Bureau of Reclamation, United States Department of the Interior, Denver, 60 p. (1998).
16. Buckingham, E. "Model experiments and the forms of empirical equations", *Trans. A.S.M.E*, **37**, pp. 263-296 (1915).
17. Lauber, G. and Hager, W.H. "Experiments to dam-break wave: Horizontal channel", *Journal of Hydraulic Research*, **36**(3), pp. 291-307 (1998).
18. Vischer, D.L. and Hager, W.H., *Dam Hydraulics*, Wiley, Chichester, UK (1998).
19. Soares-Frazão, S. and Zech, Y. "Experimental study of dambreak flow against an isolated obstacle", *Journal of Hydraulic Research*, **45**(S1), pp. 27-36 (2007).
20. Hooshyaripor, F. and Tahershamsi, A. "Effect of reservoir side slope on dam-break flood wave", *Engineering Applications of Computational Fluid Mechanics*, **9**(1), pp. 458-468 (2015).
21. Yochum, S.E., Goertz, L.A., and Jones, P.H. "Case study of the big bay dam failure: Accuracy and comparison of breach predictions", *Journal of Hydraulic Engineering*, **134**(9), pp. 1285-1293 (2008).
22. Xu, Y. and Zhang, L.M. "Breaching parameters for earth and rockfill dams", *Journal of Geotechnical and Geoenvironmental Engineering*, **135**(12), pp. 1957-1970 (2009).
23. Launder, B.E. and Spalding, D.B. "The numerical computation of turbulent flows", *Computer Methods in Applied Mechanics and Engineering*, **3**(2), pp. 269-289 (1974).
24. Mirhoseini, T.S. "Experimental study of the effect of shape factor on dam break outflow hydrograph", MSc Dissertation, Amirkabir University of Technology, Iran (2013).

Biographies

Farhad Hooshyaripor is an Assistant Professor in Civil Engineering at the Tehran Science and Research Branch of Islamic Azad University and also a post-doctoral research fellow at Amirkabir University of Technology (AUT). Dr. Hooshyaripor received his PhD in Water Engineering from AUT in 2015. His practical experience is in water resources management and flood simulation and risk management.

Ahmad Tahershamsi is an Associate Professor in the Civil and Environment Faculty, Amirkabir University of Technology. He received his PhD degree in Hydraulic Engineering from the University of Manchester in 1988 and has long time experiences in unsteady flow simulation. He has been a supervisor or advisor of many master and doctoral theses in hydraulic structures.

Sahand Razi is an MSc student in Water Resources Engineering at Islamic Azad University working on watershed planning and management. He has received his BSc degree in Civil Engineering from the Islamic Azad University in 2009.